QoE-aware Airborne Communication Infrastructure for Surveillance in Wildfires

Praveen Fernando
Department of Computer and Information Technology
Purdue University
West Lafayette, IN
ferna159@purdue.edu

Jin Wei-Kocsis
Department of Computer and Information Technology
Purdue University
West Lafayette, IN
kocsis0@purdue.edu

***Abstract*—Global warming is one of the fundamental threats to all living beings today. Various side effects are triggered as a consequence of global warming. Frequent wildfires are one of the side effects causing the loss of lives, vegetation, and economies on a significant scale each year. Therefore, sophisticated mechanisms for surveilling wildfires, including communication systems that are resilient enough to transmit surveillance information to first responders even in the presence of wildfires are urgent. In this work, we leverage unmanned aerial vehicles (UAVs), cognitive radio (CR), and deep reinforcement learning (DRL) technologies to propose a Quality of Experience (QoE)–aware airborne communication infrastructure that can deliver surveillance video streams to a destination in a disaster such as wildfire. In our simulation results, we evaluate the performance of our proposed communication infrastructure by considering different scenarios.**

***Index Terms*—Wildfires, cognitive radio, DRL, UAVs, airborne communication**

I. Introduction

The rising temperatures due to global warming and unusually warm weather are vital ingredients to fuel wildfires. Wildfires affect the health of living beings, plants, and vegetation, and severely impact economies. One such example is the recent wildfires in Maui, Hawaii, which has killed over a hundred people and is one of the deadliest wildfires in the USA. To enable an effective emergency response to wildfires, one of the urgent needs is to inform the first responders with near real-time information of wildfire progression. Considering that conventional communication systems, such as stationary ground-based communication systems are susceptible to fire damage, it is urgent to realize a resilient communication infrastructure even in the presence of wildfires [1]. To pave the path to this goal, we propose a QoE-aware airborne communication infrastructure for wildfire surveillance by employing UAV, CR, and DRL techniques.

Various research have been developed to apply UAVs and CRs for airborne communications. In [2], an airborne UAV was proposed to transmit data to secondary ground terminals (SGTs) during its flight time while minimizing disruptions to a ground-based primary network and maximizing the amount of data received by each SGT. The authors in [3] proposed a method to address the trajectory optimization of an airborne secondary relay that relays information between two ground-based secondary terminals while coexisting with a primary network. In [4], a resource allocation and trajectory planning method was proposed, where an airborne UAV maximizes the throughput of data it transmits to groud-based secondary terminals during its flight time while minimizing the disruptions to a primary network. These works only focus on optimizing the Quality of Service (QoS) of data transmission. Compelling evidence shows that, in scenarios such as wildfires where telecommunication environments tend to vary significantly, improving QoE is realistic compared to QoS. A QoE metric is typically made of several QoS metrics, and achieving a target QoE level is possible in such dynamic environments by trading off the individual QoS metrics, rather than optimizing each QoS metric individually. Therefore, the existing work on applying UAVs and CRs for airborne communications cannot be directly used for wildfire surveillance as a QoE-aware near real-time video streaming framework is needed. The authors in [5] proposed a QoE-aware video stream delivery framework, where a set of surveillance UAVs capture continuous video streams of wildfires and transmit those data to an airborne base station (BS). This is effective in providing QoE-aware traffic delivery amidst wildfires. However, in cases where wildfires spread across a vast geographical region, a single airborne BS is not sufficient in providing coverage to all the fire surveillance UAVs. To address these shortcomings, our paper provides a framework for enabling a QoE-aware video delivery framework with multiple airborne BSs providing coverage to fire surveillance UAVs. Furthermore, our work also introduces a routing functionality for airborne BSs to route the received surveillance data to a remote ground-based operator.

The rest of the paper is organized as follows. In Section II, we will present the problem formulation. In Section III, we will introduce our proposed surveillance infrastructure for wildfires. In Section IV, we will illustrate simulation results, followed by conclusions in Section V.

II. Problem Formulation

In our work, we propose a QoE-aware airborne communication infrastructure for surveillance in wildfires. An overview of our proposed communication system is illustrated in Fig. 1. As shown in the figure, our proposed communication infrastructure has a two-layer framework. To design the first layer, we assume multiple fire areas spread across a geographical region

979-8-3503-7099-7/24/$31.00 ©2024 IEEE

and consider multiple CR-integrated UAVs to surveil each fire area. For simplicity, we assume four UAVs, denoted as $\mathcal{U}_{i,1}$, $\mathcal{U}_{i,2}$, $\mathcal{U}_{i,3}$, and $\mathcal{U}_{i,4}$, surveil each fire area $i \in \{1, \cdots, \mathcal{I}\}$. These UAVs continuously capture the fire areas and transmit a video stream to a remote BS which we denote by $\mathcal{B}$. As illustrated in Fig. 1, the second layer in our work is proposed to realize the functionality of a routing layer, where $\mathcal{K}$ UAVs with high computational power route the traffic received from the first layer to $\mathcal{B}$. The environment in our work also consists of a stationary primary user (PU) denoted by $\mathcal{P}$ that transmits on a particular frequency at a given time. This frequency can vary at different time steps. Since the UAVs considered are integrated with CRs, they have the capabilities to prevent disruptions to any PU communications. There are $\mathcal{N}$ number of channels in the environment.

III. Proposed Communication Infrastructure

The overview of our proposed communication infrastructure is illustrated in Fig. 1. For simplicity, in our current work, we assume that the horizontal movement of surveillance UAVs is limited to a rectangle, as illustrated in Fig. 2. As shown in Fig. 2, the fire area has a radius of r_i. r_s is the minimum separation distance between the fire area and the UAVs. l is the maximum distance a UAV can travel along the fire center in x and y directions. Let the center of the fire area i be (x_i, y_i). Letting the position of surveillance UAV $\mathcal{U}_{i,m}$, where $m \in \{1, 2, 3, 4\}$, at time step t be $(x^t_{\mathcal{U}_{i,m}}, y^t_{\mathcal{U}_{i,m}}, z^t_{\mathcal{U}_{i,m}})$, we are able to model the position constraints of $\mathcal{U}_{i,1}, \mathcal{U}_{i,2}, \mathcal{U}_{i,3}, \mathcal{U}_{i,4}$ at t as follows:

$$
\begin{aligned}
&x_i - a \leqslant x^t_{\mathcal{U}_{i,1}} \leqslant x_i + a, y_i + a \leqslant y^t_{\mathcal{U}_{i,1}} \leqslant y_i + b, h_i \leqslant z^t_{\mathcal{U}_{i,1}} \leqslant h_{max} \\
&x_i - b \leqslant x^t_{\mathcal{U}_{i,2}} \leqslant x_i - a, y_i - a \leqslant y^t_{\mathcal{U}_{i,2}} \leqslant y_i + a, h_i \leqslant z^t_{\mathcal{U}_{i,2}} \leqslant h_{max} \\
&x_i - a \leqslant x^t_{\mathcal{U}_{i,3}} \leqslant x_i + a, y_i - b \leqslant y^t_{\mathcal{U}_{i,3}} \leqslant y_i - a, h_i \leqslant z^t_{\mathcal{U}_{i,3}} \leqslant h_{max} \\
&x_i + a \leqslant x^t_{\mathcal{U}_{i,4}} \leqslant x_i + b, y_i - a \leqslant y^t_{\mathcal{U}_{i,4}} \leqslant y_i + a, h_i \leqslant z^t_{\mathcal{U}_{i,4}} \leqslant h_{max}
\end{aligned} \tag{1}
$$

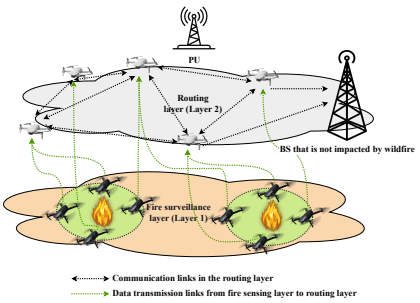

Fig. 1: Illustration of our proposed communication infrastructure.

TABLE I: Video quality-bit rate mapping [5].

Video quality	Resolution	Bit rate range
144p	256 × 144	80 ∼ 100 kbps
240p	426 × 240	300 ∼ 700 kbps
360p	640 × 360	400 ∼ 1000 kbps
480p	854 × 480	500 ∼ 2000 kbps

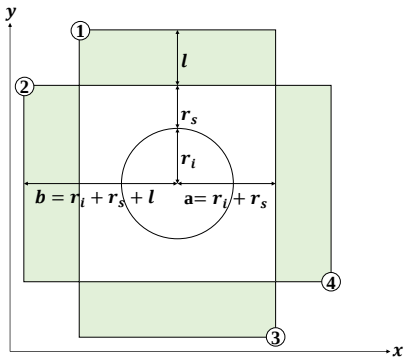

Fig. 2: Illustration of the horizontal movement of surveillance UAVs around the fire area i.

where h_i is the height of the fire i, and h_{max} is the maximum height that a UAV can fly. Letting the position of the routing UAV $\mathcal{L}_k$ at t be $(x^t_{\mathcal{L}_k}, y^t_{\mathcal{L}_k}, z^t_{\mathcal{L}_k})$, the positional constraints of $\mathcal{L}_k$ at time step t can be formulated as follows:

$$
\begin{cases}
\sqrt{(x^t_{\mathcal{L}_k} - x_j)^2 + (y^t_{\mathcal{L}_k} - y_j)^2} \geqslant a \\
\max\limits_{j}\{h_j\} \leqslant z^t_{\mathcal{L}_k} \leqslant h_{max}
\end{cases} \tag{2}
$$

where $j \in \{1, \cdots, \mathcal{I}\}$. The first condition in Eq. (2) is formulated to ensure that the routing UAVs will not get too close to the fire areas. The second condition is formulated to ensure that all the routing UAVs will fly higher than the maximum height of the fire areas. In our work, there are two BSs, $\mathcal{P}$ and $\mathcal{B}$, where $\mathcal{P}$ refers to the PU and $\mathcal{B}$ refers to the BS that is the final destination of all the video streams, as illustrated in Fig. 1. At each time step, a surveillance UAV $\mathcal{U}_{i,m}$ in Layer 1 transmits a video stream about the wildfire to a routing UAV $\mathcal{L}_k$ in Layer 2. In Layer 2, the routing UAVs route the traffic received from Layer 1 to $\mathcal{B}$. In our current work, we consider that the routing protocol employed by these UAVs is Ad-hoc On-Demand Distance Vector (AODV) routing [6]. We would like to claim that our proposed work can be generalized by considering other routing protocols.

Additionally, it is reasonable to consider that the video stream transmitted from the surveillance UAVs consists of multiple frames with variable size $r_{px} \times r_{py}$. Therefore, depending on the frame size, we consider different video qualities in the work presented in this paper. Different video qualities used in our work and the average data rate used to achieve those qualities are stated in Table I. Let the video quality of fire area i at time step t be $\mathcal{Q}^t_i$. As mentioned previously, each surveillance UAV will transmit a frame at each time step to the routing layer. Let us consider that the surveillance UAV $\mathcal{U}_{i,m}$ transmits its current frame to the routing UAV $\mathcal{L}_{\mathcal{U}^d_{i,m}}$ over the channel $\mathcal{C}_{\mathcal{U}^c_{i,m}}$. Routing UAV and channel selection of $\mathcal{U}_{i,m}$ should satisfy $\sum_{k=1}^{\mathcal{K}} \mathbf{I}_1(k) = 1$, and $\sum_{n=1}^{\mathcal{N}} \mathbf{I}_2(n) = 1$, where $\mathbf{I}_1(k) = 1$ if $k = \mathcal{U}^d_{i,m}$ and $\mathbf{I}_1(k) = 0$ otherwise, and $\mathbf{I}_2(n) = 1$ if $n = \mathcal{U}^c_{i,m}$, and $\mathbf{I}_2(n) = 0$ otherwise. $\mathcal{U}_{i,m}$ also chooses the receiving channel of $\mathcal{B}$ as $\mathcal{C}_{\mathcal{U}^{c'}_{i,m}}$. In other words, $\sum_{n=1}^{\mathcal{N}} \mathbf{I}_3(n) = 1$, where $\mathbf{I}_3(n) = 1$ if

$n = \mathcal{U}_{i,m}^{c'}$, and $\mathbf{I}_3(n) = 0$ otherwise. Here, $\mathbf{I}_1(\cdot)$, $\mathbf{I}_2(\cdot)$, and $\mathbf{I}_3(\cdot)$ are indicator functions. The received datarate from $\mathcal{U}_{i,m}$ to $\mathcal{B}$ at t is $\mathcal{R}^t_{\mathcal{U}_{i,m}}$. Let the time taken to transmit a frame from $\mathcal{U}_{i,m}$ to $\mathcal{B}$ at time step t be $\mathcal{T}^t_{i,m}$. Therefore, the maximum time taken to receive all the frames at $\mathcal{B}$ at t is $\mathcal{T}^t_{max} = \max_{i,m}\{\mathcal{T}^t_{i,m}\}$ where $i \in \{1, \ldots, \mathcal{I}\}$, and $m \in \{1, 2, 3, 4\}$.

A. Path loss models

To model the path losses in our work, we need to take into account the spatial diversity of different components in our proposed work. Therefore, we leverage path loss models that cover both air and ground communications based on the work in [7].

1) Air to air model: The communication between two UAVs can be formulated via an exponential decaying path loss model [7]. Furthermore, as stated in [8], Rayleigh fading coefficient is formulated as $h = \sigma(\mathcal{N}(0,1) + j\mathcal{N}(0,1))$, where $\sigma^2 = \frac{1}{2}$ and $\mathcal{N}(0,1)$ denotes standard normal distribution. Additionally, it is reasonable to assume that the communication between two UAVs is line-of-sight (LOS), and thus we can formulate the Rician coefficient by adding the LOS component to the Rayleigh fading coefficient. Therefore, h for the Rican fading coefficient can be formulated as $h = 1 + \sigma(\mathcal{N}(0,1) + j\mathcal{N}(0,1))$ where $\sigma^2 = \frac{1}{2}$. Ultimately, we realize the modeling of the UAV-to-UAV communications by using Rician fast fading along with exponentially decaying loss function. Then, the received power from UAV γ_2 to γ_1 can be formulated as $P^{\mathcal{R}}_{\gamma_1} = P^{\mathcal{T}}_{\gamma_2} G d(\gamma_1, \gamma_2)^{-\alpha} |h|^2$, where UAVs γ_1 and γ_2 can be two routing UAVs, or one routing UAV and one surveillance UAV, respectively, G is the channel gain, α denotes the path loss exponent, and $d(\gamma_1, \gamma_2)$ is a function used to find the Euclidean distance between UAVs γ_1 and γ_2.

2) Ground to ground model: To formulate the ground-to-ground communication between $\mathcal{P}$ and $\mathcal{B}$, we leverage the model proposed in [7] to model the path loss between two BSs γ_1 and γ_2 as $PL^{\mathbf{dB,BS-BS}}_{\gamma_1,\gamma_2} = -55.9 + 38\log_2(d(\gamma_1,\gamma_2)) + \left(24.5 + \frac{1.5\mathcal{F}}{925}\right)\log_2(\mathcal{F})$. Based on the formulation, the received power from $\mathcal{P}$ to $\mathcal{B}$ can be calculated as $P^{\mathcal{R}}_{\mathcal{B}} = \frac{P^{\mathcal{T}}_{\mathcal{P}}}{10^{PL^{\mathbf{dB,BS-BS}}_{\mathcal{P},\mathcal{B}}/10}}$.

3) Air to ground model: The average path loss between a UAV γ_2 and a BS γ_1 can be modeled in dB as $PL^{\mathbf{dB,BS-UAV}}_{\gamma_2,\gamma_1} = P^{\mathbf{LOS}}_{\gamma_2,\gamma_1} \cdot PL^{\mathbf{LOS}}_{\gamma_2,\gamma_1} + P^{\mathbf{NLOS}}_{\gamma_2,\gamma_1} \cdot PL^{\mathbf{NLOS}}_{\gamma_2,\gamma_1}$, where $P^{\mathbf{LOS}}_{\gamma_2,\gamma_1} = 1 - P^{\mathbf{NLOS}}_{\gamma_2,\gamma_1}$, and $P^{\mathbf{LOS}}_{\gamma_2,\gamma_1}$, $PL^{\mathbf{LOS}}_{\gamma_2,\gamma_1}$, and $PL^{\mathbf{NLOS}}_{\gamma_2,\gamma_1}$ are given as follows:

$$\begin{cases} P^{\mathbf{LOS}}_{\gamma_2,\gamma_1} & = \frac{1}{1 + ae^{(-b(\delta_{\gamma_2,\gamma_1} - a))}} \\ PL^{\mathbf{LOS}}_{\gamma_2,\gamma_1} & = 20\log_2(\mathcal{F}) + 20\log_2\left(\frac{4\pi}{c}\right) + 20\log_2(d(\gamma_2,\gamma_1)) + \eta^{\mathbf{LOS}} \\ PL^{\mathbf{NLOS}}_{\gamma_2,\gamma_1} & = 20\log_2(\mathcal{F}) + 20\log_2\left(\frac{4\pi}{c}\right) + 20\log_2(d(\gamma_2,\gamma_1)) + \eta^{\mathbf{NLOS}} \end{cases} \tag{3}$$

where $\delta_{\gamma_2,\gamma_1} = \sin^{-1}\left(\frac{h(\gamma_2) - h(\gamma_1)}{d(\gamma_2,\gamma_1)}\right)$ and $h(\cdot)$ is a function to calculate the height of an object. Then, the received power from γ_2 to γ_1 can be stated as $P^{\mathcal{R}}_{\gamma_1} = \frac{P^{\mathcal{T}}_{\gamma_2}}{10^{PL^{\mathbf{dB,BS-UAV}}_{\gamma_2,\gamma_1}/10}}$, where γ_1 and γ_2 can be the BS $\mathcal{B}$ and a routing UAV, respectively, or the PU $\mathcal{P}$ and a UAV (i.e., routing or surveillance UAV), respectively.

B. Co-existence with PUs

In this work, we consider that all UAVs and the BS $\mathcal{B}$ have spectrum-sensing capabilities by following a spectrum overlay co-existence strategy. At the beginning of each time slot, each UAV will perform spectrum sensing to identify any active PU communications and turn off the radio interface where the active communication is detected. Furthermore, $\mathcal{B}$ also has the spectrum sensing capabilities. It will turn off the radio interface, in which the PU is active, at the beginning of each time slot. This strategy aims to discourage routing UAVs to send data to $\mathcal{B}$ when there's already interference at $\mathcal{B}$ from $\mathcal{P}$.

C. QoE-aware communication

Our proposed airborne communication infrastructure is designed to optimize QoE for enabling smooth and near real-time video streaming for surveillance of wildfires. To achieve this goal, we propose to minimize the successive throughput variation while maximizing the throughput of each surveillance UAV. Additionally, we also aim to ensure the maximum delay of the system at each step does not exceed a certain threshold. To achieve this, the model of the overall QoE of the communication infrastructure at time step t can be formulated as:

$$QoE = \theta\left(\sum_{i=1}^{\mathcal{I}}\sum_{m=1}^{4}\mathcal{R}^t_{\mathcal{U}_{i,m}} - |\mathcal{R}^t_{\mathcal{U}_{i,m}} - \mathcal{R}^{t-1}_{\mathcal{U}_{i,m}}|\right) - \omega \cdot \mathcal{D}^t \tag{4}$$

where, $|\mathcal{R}^t_{\mathcal{U}_{i,m}} - \mathcal{R}^{t-1}_{\mathcal{U}_{i,m}}|$ is formulated for minimizing throughput variation of UAV $\mathcal{U}_{i,m}$ at time step t. $\mathcal{D}^t = \mathcal{T}^t_{max} - \overline{\mathcal{T}}$ is formulated for ensuring maximum delay does not exceed the delay threshold $\overline{\mathcal{T}}$, and θ and ω are coefficients.

D. Overall optimization formulation for our proposed communication infrastructure

To achieve the objective function described in Eq. (4), each surveillance UAV will adaptively optimize its transmission power, intermediate routing UAV, intermediate channel, destination channel, and position. Furthermore, the video quality for each fire area at each time step is adaptively determined. To adjust UAV positions, each UAV determines changes on its coordinates. If the UAV γ determines the change on its position at time step t as $(\Delta x^t_\gamma, \Delta y^t_\gamma, \Delta z^t_\gamma)$, then its position at t is $(x^{t-1}_\gamma, y^{t-1}_\gamma, z^{t-1}_\gamma) + (\Delta x^t_\gamma, \Delta y^t_\gamma, \Delta z^t_\gamma) \rightarrow (x^t_\gamma, y^t_\gamma, z^t_\gamma)$. We can formulate the overall optimization problem as follows:

$$\begin{aligned} \max_{\rho} \quad & \theta\left(\sum_{i=1}^{\mathcal{I}}\sum_{m=1}^{4}\mathcal{R}^t_{\mathcal{U}_{i,m}} - |\mathcal{R}^t_{\mathcal{U}_{i,m}} - \mathcal{R}^{t-1}_{\mathcal{U}_{i,m}}|\right) - \omega \cdot \mathcal{D}^t \\ \text{subject to} \quad & \sum_{k=1}^{\mathcal{K}} \mathbf{I}_1(k) = 1 \\ & \sum_{n=1}^{\mathcal{N}} \mathbf{I}_2(n) = 1 \\ & \sum_{n=1}^{\mathcal{N}} \mathbf{I}_3(n) = 1 \\ & P_{min} \leqslant P^{\mathcal{T}}_{\mathcal{L}_k}, P^{\mathcal{T}}_{\mathcal{U}_{i,m}} \leqslant P_{max} \\ & \text{Positional constraints in Eqs. (1) and (2)} \end{aligned} \tag{5}$$

where $\rho = \mathcal{L}_{\mathcal{U}^d_{i,m}}$, $\mathcal{C}_{\mathcal{U}^c_{i,m}}$, $P^{\mathcal{T}}_{\mathcal{U}_{i,m}}$, $\mathcal{Q}^t_i$, $\mathcal{C}_{\mathcal{U}^{c'}_{i,m}}$, $\Delta x^t_{\mathcal{U}_{i,m}}$, $\Delta y^t_{\mathcal{U}_{i,m}}$, $\Delta z^t_{\mathcal{U}_{i,m}}$, $\Delta x^t_{\mathcal{L}_k}$, $\Delta y^t_{\mathcal{L}_k}$, $\Delta z^t_{\mathcal{L}_k}$, $P^{\mathcal{T}}_{\mathcal{L}_k}$, $i \in \{1, \ldots, \mathcal{I}\}$, $m \in \{1, 2, 3, 4\}$, and $k \in \{1, \cdots, \mathcal{K}\}$.

E. DRL-enabled optimization realization

Considering that the optimization model in Eq. (5) has high complexity and one type of emerging machine learning techniques, DRLs, have demonstrated powerful capabilities in solving complex optimization problems, in our work, we exploit DRL techniques to deploy our proposed optimization model for communication management. We propose to model the procedure of determining the transmission and spatial parameters based on the environment state as a Markov Decision Process (MDP). Additionally, considering our optimization model involves a combination of continuous and discrete action space, we leverage one type of DRL technique, the Deep Deterministic Policy Gradient (DDPG) method in our work. To achieve our optimization goal, we consider the objective function stated in Eq. (5) as the DRL reward function to evaluate and optimize the decision-making of the routing and surveillance UAVs. Furthermore, we can define the state and action of the DRL algorithm as follows:

$$\begin{aligned} s_t &= [\overline{\mathcal{Q}^{t-1}}, \overline{\mathbf{POS}^{t-1}_{\mathcal{U}}}, \overline{\mathbf{POS}^{t-1}_{\mathcal{L}}}, \overline{\mathcal{R}^{t-1}}, \mathcal{T}^{t-1}_{max}, \overline{\mathbf{SS}^t_{\mathcal{U}}}, \overline{\mathbf{SS}^t_{\mathcal{L}}}, \mathbf{SS}^t_{\mathcal{B}}] \\ a_t &= [\overline{\mathcal{L}_{\mathcal{U}^d}}, \overline{\mathcal{L}_{\mathcal{U}^c}}, \overline{\mathcal{L}_{\mathcal{U}^{c'}}}, \overline{P^{\mathcal{T}}_{\mathcal{U}}}, \overline{P^{\mathcal{T}}_{\mathcal{L}}}, \overline{\Delta\mathbf{POS}^t_{\mathcal{U}}}, \overline{\Delta\mathbf{POS}^t_{\mathcal{L}}}, \overline{\mathcal{Q}^t}] \end{aligned} \tag{6}$$

where $\overline{\mathcal{Q}^t}$ is the vector of the video quality of each fire area at time step t. $\overline{\mathbf{POS}^{t-1}_{\mathcal{U}}}$ is the position of surveillance UAVs at time step $t-1$, and $\overline{\mathbf{POS}^{t-1}_{\mathcal{L}}}$ is the position of routing UAVs at time step $t-1$. $\overline{\mathcal{R}^{t-1}}$ is the throughput of surveillance UAVs at time step $t-1$. $\overline{\mathcal{L}_{\mathcal{U}^d}}$ is the intermediate routing UAV selection of each surveillance UAV at t. $\overline{\mathcal{L}_{\mathcal{U}^c}}$ is the intermediate channel selection of each surveillance UAV at t. Similarly, $\overline{\mathcal{L}_{\mathcal{U}^{c'}}}$ is the destination channel selection of each surveillance UAV at t. $\overline{P^{\mathcal{T}}_{\mathcal{U}}}$ is the transmission power vector of each surveillance UAV, and $\overline{P^{\mathcal{T}}_{\mathcal{L}}}$ is the transmission power vector of the routing UAVs. $\overline{\Delta\mathbf{POS}^t_{\mathcal{U}}}$ is the position changes of the surveillance UAVs at time step t, and $\overline{\Delta\mathbf{POS}^t_{\mathcal{L}}}$ is the position changes for routing UAVs at time step t. These vector variables are defined as follows:

$$\begin{cases} \overline{\mathcal{L}_{\mathcal{U}^d}} &= [\mathcal{L}_{\mathcal{U}^d_{1,1}}, \cdots, \mathcal{L}_{\mathcal{U}^d_{1.4}}, \cdots, \mathcal{L}_{\mathcal{U}^d_{\mathcal{I},1}}, \cdots, \mathcal{L}_{\mathcal{U}^d_{\mathcal{I},4}}] \\ \overline{\mathcal{L}_{\mathcal{U}^c}} &= [\mathcal{L}_{\mathcal{U}^c_{1,1}}, \cdots, \mathcal{L}_{\mathcal{U}^c_{1.4}}, \cdots, \mathcal{L}_{\mathcal{U}^c_{\mathcal{I},1}}, \cdots, \mathcal{L}_{\mathcal{U}^c_{\mathcal{I},4}}] \\ \overline{\mathcal{L}_{\mathcal{U}^{c'}}} &= [\mathcal{L}_{\mathcal{U}^{c'}_{1,1}}, \cdots, \mathcal{L}_{\mathcal{U}^{c'}_{1.4}}, \cdots, \mathcal{L}_{\mathcal{U}^{c'}_{\mathcal{I},1}}, \cdots, \mathcal{L}_{\mathcal{U}^{c'}_{\mathcal{I},4}}] \\ \overline{P^{\mathcal{T}}_{\mathcal{U}}} &= [P^{\mathcal{T}}_{\mathcal{U}_{1,1}}, \cdots, P^{\mathcal{T}}_{\mathcal{U}_{1,4}}, \cdots, P^{\mathcal{T}}_{\mathcal{U}_{\mathcal{I},1}}, \cdots, P^{\mathcal{T}}_{\mathcal{U}_{\mathcal{I},4}}] \\ \overline{P^{\mathcal{T}}_{\mathcal{L}}} &= [P^{\mathcal{T}}_{\mathcal{L}_1}, \cdots, P^{\mathcal{T}}_{\mathcal{L}_{\mathcal{K}}}] \\ \overline{\Delta\mathbf{POS}^t_{\mathcal{U}}} &= [\Delta x^t_{\mathcal{U}_{1,1}}, \Delta y^t_{\mathcal{U}_{1,1}}, \Delta z^t_{\mathcal{U}_{1,1}}, \cdots, \Delta x^t_{\mathcal{U}_{\mathcal{I},4}}, \Delta y^t_{\mathcal{U}_{\mathcal{I},4}}, \Delta z^t_{\mathcal{U}_{\mathcal{I},4}}] \\ \overline{\Delta\mathbf{POS}^t_{\mathcal{L}}} &= [\Delta x^t_{\mathcal{L}_1}, \Delta y^t_{\mathcal{L}_1}, \Delta z^t_{\mathcal{L}_1}, \cdots, \Delta x^t_{\mathcal{L}_{\mathcal{K}}}, \Delta y^t_{\mathcal{L}_{\mathcal{K}}}, \Delta z^t_{\mathcal{L}_{\mathcal{K}}}] \\ \overline{\mathcal{Q}^t} &= [\mathcal{Q}^t_1, \cdots, \mathcal{Q}^t_{\mathcal{I}}] \\ \overline{\mathbf{POS}^{t-1}_{\mathcal{U}}} &= [x^{t-1}_{\mathcal{U}_{1,1}}, y^{t-1}_{\mathcal{U}_{1,1}}, z^{t-1}_{\mathcal{U}_{1,1}}, \cdots, x^{t-1}_{\mathcal{U}_{\mathcal{I},4}}, y^{t-1}_{\mathcal{U}_{\mathcal{I},4}}, z^{t-1}_{\mathcal{U}_{\mathcal{I},4}}] \\ \overline{\mathbf{POS}^{t-1}_{\mathcal{L}}} &= [x^{t-1}_{\mathcal{L}_1}, y^{t-1}_{\mathcal{L}_1}, z^{t-1}_{\mathcal{L}_1}, \cdots, x^{t-1}_{\mathcal{L}_{\mathcal{K}}}, y^{t-1}_{\mathcal{L}_{\mathcal{K}}}, z^{t-1}_{\mathcal{L}_{\mathcal{K}}}] \\ \overline{\mathcal{R}^{t-1}} &= [\mathcal{R}^{t-1}_{\mathcal{U}_{1,1}}, \cdots, \mathcal{R}^{t-1}_{\mathcal{U}_{\mathcal{I},4}}] \end{cases} \tag{7}$$

TABLE II: Simulation parameters

Parameters	Values
Transmission gain	15 dB
P_{min}	16.0206 dBm
P_{max}	31.0206 dBm
Reception gain	35 dB
θ	1
ω	0.1
r_i	250 m [5]
r_s	9 m [9]
l	10 m
h_{max}	100 m [5]
Height of $\mathcal{P}, \mathcal{B}$	30 m [10]
α	2 [7]
G	$10^{-3.15}$ or $(-31.5\,dB)$ [7]
a	12
b	0.135
η^{LOS}	1
η^{NLOS}	20

Furthermore, $\overline{\mathbf{SS}^t_{\mathcal{U}}}$ is a vector consisting of spectrum sensing results of surveillance UAVs, and $\overline{\mathbf{SS}^t_{\mathcal{L}}}$ is a vector consisting of spectrum sensing results of routing UAVs. If the surveillance UAV $\mathcal{U}_{i,m}$ senses a PU present on channel n, we can denote this as $\mathbf{SS}^t_{\mathcal{U}^n_{i,m}} = 1$, otherwise $\mathbf{SS}^t_{\mathcal{U}^n_{i,m}} = 0$. Similarly, if the routing UAV k senses a PU present on channel n, we can denote this as $\mathbf{SS}^t_{\mathcal{L}^n_k} = 1$, otherwise $\mathbf{SS}^t_{\mathcal{L}^n_k} = 0$. $\mathbf{SS}^t_{\mathcal{B}}$ is the spectrum sensing result of $\mathcal{B}$ at t. We can denote $\overline{\mathbf{SS}^t_{\mathcal{U}}}$ and $\overline{\mathbf{SS}^t_{\mathcal{L}}}$ as follows:

$$\begin{aligned} \overline{\mathbf{SS}^t_{\mathcal{U}}} &= [\mathbf{SS}^t_{\mathcal{U}^1_{1,1}}, \cdots, \mathbf{SS}^t_{\mathcal{U}^{\mathcal{N}}_{1,1}}, \cdots, \mathbf{SS}^t_{\mathcal{U}^1_{\mathcal{I},4}}, \cdots, \mathbf{SS}^t_{\mathcal{U}^{\mathcal{N}}_{\mathcal{I},4}}] \\ \overline{\mathbf{SS}^t_{\mathcal{L}}} &= [\mathbf{SS}^t_{\mathcal{L}^1_1}, \cdots, \mathbf{SS}^t_{\mathcal{L}^{\mathcal{N}}_1}, \cdots, \mathbf{SS}^t_{\mathcal{L}^1_{\mathcal{K}}}, \cdots, \mathbf{SS}^t_{\mathcal{L}^{\mathcal{N}}_{\mathcal{K}}}] \end{aligned} \tag{8}$$

IV. Simulation Results

We leverage NS-3, which is a widely used network simulator, to conduct the simulations for evaluating the performance of our proposed airborne communication infrastructure. Throughout our simulation results, we consider an environment consisting of three fire areas, where each fire area is surveilled by 4 surveillance UAVs. Additionally, there

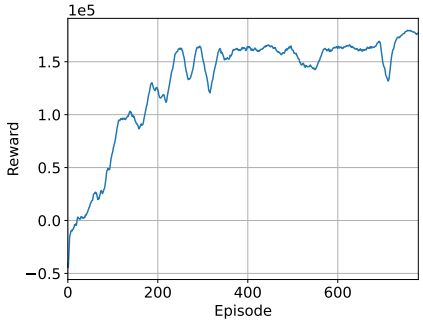

Fig. 3: Reward of our proposed communication infrastructure during training.

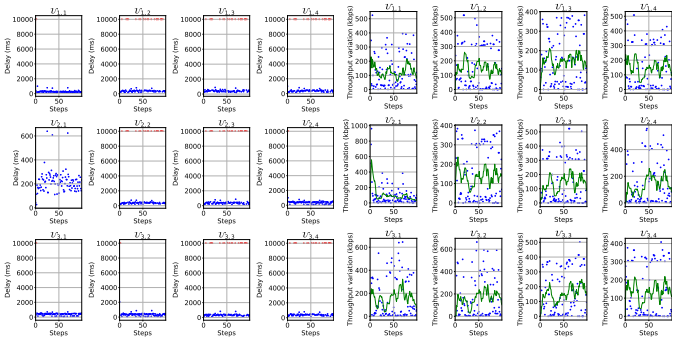

(a) Individual delays

(b) Individual throughput variations

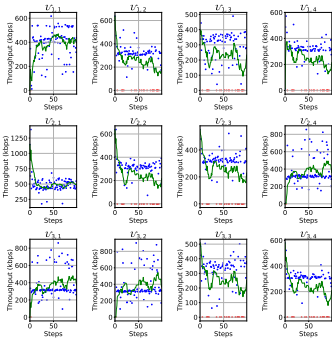

(c) Individual throughputs

Fig. 4: Performance of individual surveillance UAVs (blue dots represent successful frame receptions, red dots represent frame losses, and green lines represent the moving average of each performance metric).

are 5 routing UAVs. We consider a geographical area of $2000\,\mathrm{m} \times 2000\,\mathrm{m}$. The fire areas are arbitrarily placed in the geographical area. At the start of each episode, each routing UAV is placed at the center of the geographical area. Furthermore, $\mathcal{B}$ and $\mathcal{P}$ are placed arbitrarily in the environment. Additionally, the wireless environment consists of four channels with center frequencies of $2000\,\mathrm{MHz}, 3000\,\mathrm{MHz}, 4000\,\mathrm{MHz}, 5000\,\mathrm{MHz}$, respectively. To enable operating on different center frequencies, we set each UAV, $\mathcal{B}$, and $\mathcal{P}$ with 4 radio interfaces. Besides the spatial parameters mentioned in Section III, all the UAVs can ascend or descend $50\,\mathrm{m}$ at each step of the episode. Furthermore, they can move $25\,\mathrm{m}$ horizontally. Other simulation parameters are detailed in Table II.

Fig. 3 illustrates the total reward variation during DRL training. From Fig. 3, it is clear that the total reward increases as the training progresses. Fig. 4 illustrates the performance of individual surveillance UAVs for a single episode consisting of 100 steps. In Fig. 4(a), we can observe the delay of the individual UAVs. In some UAVs, we can observe some frame losses characterized by a high value of delay (identified by red scatters). However, the majority of the delay values are low. Fig. 4(b), and 4(c) show individual throughput variation and throughput, respectively. From Fig. 4(b), we can see that our proposed method enables the system to maintain the average throughput variation at a low level that varies approximately between 50 to $250\,\mathrm{kbps}$. As shown in Fig. 4(c), the average throughput is in the range from 200 to $600\,\mathrm{kbps}$, which is a relatively moderate range. This is reasonable since our proposed QoE-aware multi-objective optimization model for airborne communication infrastructure aims to achieve a tradeoff amongst maximizing the throughput, enforcing the maximum delay at a low level, and minimizing throughput variation. In our ongoing work, we are exploring appropriate strategies to enable an optimal tradeoff between high throughput, low throughput variation, and low maximum delay.

V. Conclusions

In this work, we propose a QoE-aware airborne communication infrastructure for scalable surveillance of wildfires. Our proposed communication infrastructure has a two-layer hierarchical framework, where the first layer consists of fire surveillance UAVs and the second layer consists of routing UAVs that receive surveillance video streams from the first layer and routes them to the destination BS. Simulation results illustrate that our proposed communication infrastructure is effective in ensuring QoE requirements for delivering video streams for wildfire surveillance. In our ongoing work, we are improving our proposed communication infrastructure to further optimize QoE metrics. Additionally, we are exploring appropriate strategies to carry out in-field experiments.

References

[1] Federal Communications Commission, "Wildfire Communications Advisory." [Online]. Available: https://tinyurl.com/4p5mu8cc

[2] S. K. Nobar, M. H. Ahmed, Y. Morgan, and S. A. Mahmoud, "Resource Allocation in Cognitive Radio-Enabled UAV Communication," *IEEE Transactions on Cognitive Communications and Networking*, vol. 8, no. 1, pp. 296–310, 2022.

[3] Z. Wang, F. Zhou, Y. Wang, and Q. Wu, "Joint 3D trajectory and resource optimization for a UAV relay-assisted cognitive radio network," *China Communications*, vol. 18, no. 6, pp. 184–200, 2021.

[4] Y. Pan, X. Da, H. Hu, Y. Huang, M. Zhang, K. Cumanan, and O. A. Dobre, "Joint Optimization of Trajectory and Resource Allocation for Time-Constrained UAV-Enabled Cognitive Radio Networks," *IEEE Transactions on Vehicular Technology*, vol. 71, no. 5, pp. 5576–5580, 2022.

[5] L. A. b. Burhanuddin, X. Liu, Y. Deng, U. Challita, and A. Zahemszky, "QoE Optimization for Live Video Streaming in UAV-to-UAV Communications via Deep Reinforcement Learning," *IEEE Transactions on Vehicular Technology*, vol. 71, no. 5, pp. 5358–5370, 2022.

[6] C. E. Perkins and E. M. Royer, "Ad-hoc on-demand distance vector routing," in *Proceedings WMCSA'99. Second IEEE Workshop on Mobile Computing Systems and Applications*, 1999, pp. 90–100.

[7] S. Zhang, H. Zhang, B. Di, and L. Song, "Cellular UAV-to-X Communications: Design and Optimization for Multi-UAV Networks," *IEEE Transactions on Wireless Communications*, vol. 18, no. 2, pp. 1346–1359, 2019.

[8] L. Yan, Z. Qin, R. Zhang, Y. Li, and G. Y. Li, "Resource Allocation for Text Semantic Communications," *IEEE Wireless Communications Letters*, vol. 11, no. 7, pp. 1394–1398, 2022.

[9] National Agroforestry Center (U.S. Department of Agriculture), "Conservation Buffers." [Online]. Available: https://tinyurl.com/27m8zk5j

[10] Federal Communications Commission, "Human Exposure to Radio Frequency Fields: Guidelines for Cellular Antenna Sites." [Online]. Available: https://tinyurl.com/nhhkwzsf